ACS APPLIED ELECTRONIC MATERIALS

Article

Cite This: ACS Appl. Electron. Mater. 2019, 1, 2455−2462

pubs.acs.org/acsaelm

UV−Ozone Modified Sol−Gel Processed ZnO for Improved Diketopyrrolopyrrole-Based Hybrid Photodetectors

Alec Pickett,[†] Aiswarya A. Mohapatra,[‡] Suman Ray,[‡,∥] Qiangsheng Lu,[†] Guang Bian,[†] Kartik Ghosh,[§] Satish Patil,[‡] and Suchismita Guha*[,†]

[†]Department of Physics and Astronomy, University of Missouri, Columbia, Missouri 65211, United States

[‡]Solid State and Structural Chemistry Unit, Indian Institute of Science, Bangalore 560012, India

[§]Department of Physics, Astronomy, and Materials Science, Missouri State University, Springfield, Missouri 65897, United States

ABSTRACT: Organic−inorganic interfaces in photodiodes have recently gathered significant interest due to the realization of intrinsic p−n junctions and unique physical properties. Nanopatterned sol−gel ZnO films provide an alternate path for fullerene-free organic photodetectors. However, naturally occurring oxygen vacancies in ZnO often act as trap sites and can degrade device performance if left unchecked. Here, we focus on the role of UV−ozone treatment for filling oxygen vacancies in sol−gel processed ZnO for improving the hybrid interface with thienothiophene linked diketopyrrolopyrrole (DPP) films. The ZnO films are characterized by X-ray diffraction, ultraviolet photoelectron spectroscopy (UPS), cross-sectional electron microscope images, and electron energy loss spectroscopy (EELS). UV−ozone treatment shows no change in the crystal structure, but UPS indicates that the treated films are more resistive and have a higher oxygen concentration at the surface. The EELS spectra show gradual passivation of oxygen vacancies within the bulk of the ZnO films. Fullerene-free photodetectors fabricated from ZnO:DPP interfaces show dark currents reduced by half and photoresponsivities nearly doubled, on average, when the ZnO surface is UV−ozone treated compared to nontreated ZnO films, indicating this simple technique to be excellent for improving photodiode performance when ZnO is used as an electron transport layer.

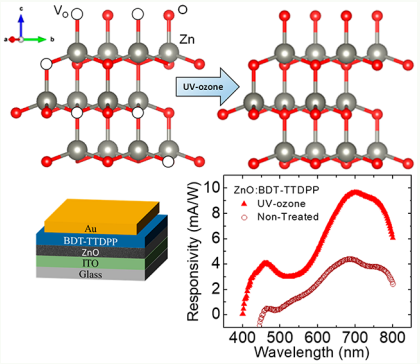

KEYWORDS: *ZnO, donor−acceptor copolymer, photodiode, UV−ozone, sol−gel, defects*

1. INTRODUCTION

The intrinsic n-type nature of ZnO makes it a favorable semiconductor to interface with p-type π-conjugated molecules and polymers for the formation of p−n junctions. Such hybrid interfaces have found ubiquitous applications in solar cells[1−4] and photodiodes, light-emitting diodes,[5,6] and thin film transistors.[7] ZnO was one of the first oxide semiconductors to be used in dye-sensitized solar cells[8] after it was shown in the early 1970s that excited chlorophyll molecules can inject electrons to the conduction band of ZnO, resulting in an anodic photocurrent.[9] Since ZnO is nontoxic, has high exciton binding energy, and is a wide band gap semiconductor, it is an excellent material for optoelectronic applications.[10,11] Another attractive feature of ZnO is that it can be synthesized in a large variety of nanostructures, from nanoparticles to hierarchical structures,[8,12] using a variety of deposition methods such as atomic layer deposition (ALD), pulsed laser deposition, hydrothermal deposition, spray pyrolysis, chemical vapor deposition, and sol−gel processing. Such nanostructures are particularly useful in interfacing with p-type materials for increasing the interfacial area. In addition, ZnO is often used as a buffer layer for electron transport in bulk heterojunction (BHJ) solar cells.[13,14] Increasing the interfacial area in these BHJ devices has also helped improve charge collection.[2,3,15,16] Furthermore, doped ZnO films enhance UV stability in polymer solar cells.[17]

Through solution processing and solvent annealing it has been shown that ZnO films can form nanoridges; when used in inverted bulk heterojunction polymer solar cells (with P3HT:PCBM), such films improved the power conversion efficiency by 25% compared to using only planar films with ZnO nanoparticles.[16] Nanostructured ZnO films provide an alternate pathway for the fabrication of polymer photodiodes and solar cells without the use of fullerenes. However, sol−gel processed ZnO films are not entirely without faults. Naturally occurring defects in ZnO might occur as oxygen vacancies, as zinc vacancies, as zinc and oxygen interstitials, or as antisites.[18] Although oxygen vacancies have been shown to enhance photocatalytic performance,[11] it may be detrimental to transport in photodiode architectures as vacancies may act as recombination sites. It has been demonstrated in theoretical and experimental work that the oxygen vacancies (V_O) are closely related to electronic structure, charge transport, and various optical and surface properties. These vacancies can

Received: September 13, 2019
Accepted: October 30, 2019
Published: October 30, 2019

DOI: 10.1021/acsaelm.9b00597
ACS Appl. Electron. Mater. 2019, 1, 2455−2462

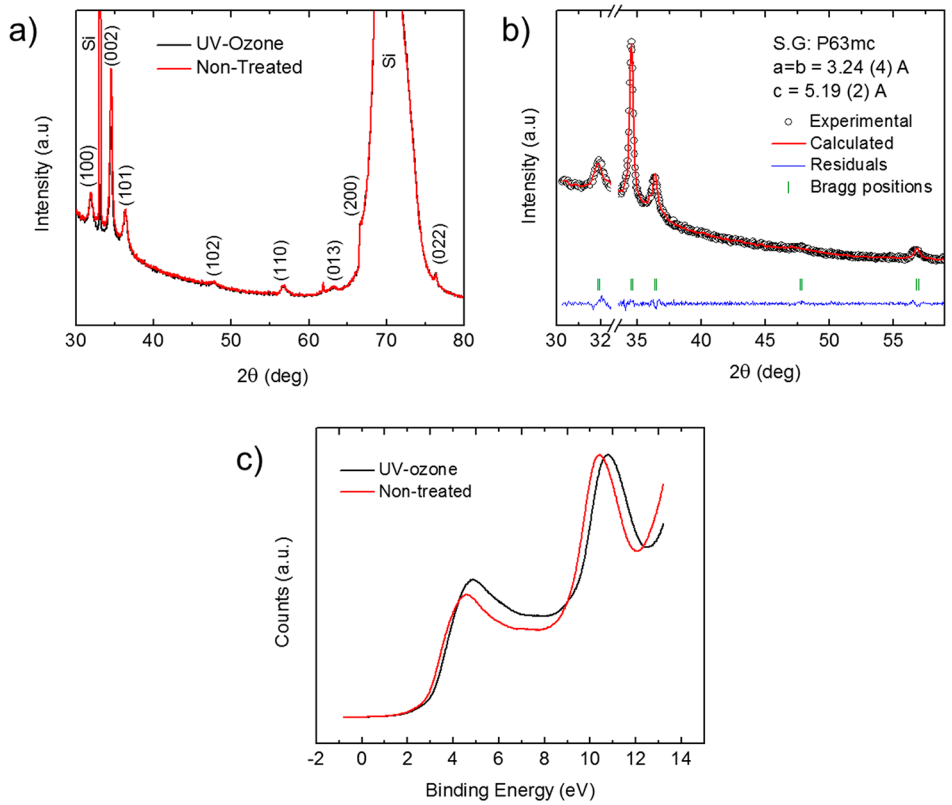

Figure 1. (a) XRD from UV−ozone treated and nontreated ZnO films on Si substrates with indexed planes. (b) Le Bail fit of the XRD data showing the ZnO films have a hexagonal wurtzite structure with space group and lattice constants indicated. The break in the *x*-axis omits the Si peak. (c) UPS spectra of UV−ozone and nontreated ZnO films, showing a small shift of the valence band edge toward higher binding energy for the UV−ozone treated sample.

result in isolated energy levels which enhance reaction processes and optical absorption in the visible region.[11] Thermal annealing in air is one way to decrease the concentration of oxygen vacancies in ZnO.[19] Surface modifications of ZnO films by using a thin ALD grown ZnO on nanostructured ZnO films,[20] UV light soaking,[21] and UV−ozone treatment[22,23] have also been shown to reduce oxygen vacancies.

Although the field of infrared and near-infrared photodetectors has mainly relied on III−V semiconductors, solution processed conjugated polymers and oligomers based on donor−acceptor moieties, hybrid organic halide perovskites, and colloidal quantum dots are emerging as next-generation photodetectors, offering band gap tunability with high photogeneration efficiencies.[24] Donor−acceptor copolymers based on diketopyrrolopyrrole (DPP) cores have garnered much attention in red and near-infrared photodiodes and solar cells[25−27] as well as in field-effect transistors where they show ambipolar transport with relatively high carrier mobilities and good air stability.[28−33] In a prior study, it was seen that the linking unit between the acceptor DPP core and the benzodithiophene (BDT) donor plays a decisive role in the charge dissociation process and carrier mobilities. BDT-TTDPP, which has a thienothiophene linking unit, showed 2 orders of magnitude higher photoresponsivity in photodiode architectures using ZnO as the n-type layer when compared to BDT-TDPP, which has a thiophene linking unit. The thienothiophene linker between the donor and acceptor units in BDT-TTDPP enhances backbone planarity and thus the overall charge transport characteristics.[34]

In this study, we explore the effect of oxygen vacancies in nanopatterned ZnO films and how a UV−ozone treatment fills these vacancies to improve photodiode performance. X-ray diffraction measurements determine no change in structure between UV−ozone treated and nontreated films. Electron energy loss spectroscopy (EELS) and ultraviolet photoelectron spectroscopy (UPS) are used to determine the relative oxygen concentration and the changes in the valence band edge. Cross-sectional electron microscopy images show that crystallographic structure takes no preferred growth direction and remains unchanged upon UV−ozone treatment. The treated ZnO films were used in fullerene-free DPP-based photodiodes, where the overall performance is seen to significantly improve compared with nontreated ZnO films.

2. EXPERIMENTAL METHODS

2.1. Materials. ZnO films were spin-cast on ITO-coated glass, which was obtained from Ossila, in addition to glass coverslips and encapsulation epoxy. The ITO films are 100 nm thick with an RMS surface roughness of 1.8 nm. Zinc acetate dihydrate ($C_4H_6O_4Zn\cdot 2H_2O$, ACS Reagent ≥ 98%), ethanolamine (C_2H_7NO, ACS Reagent ≥ 99.0%), and 2-methoxyethanol ($C_3H_8O_2$, anhydrous 99.8%) used in fabricating the ZnO precursor solution were each acquired from Sigma-Aldrich. The solvents, 1,2-dichlorobenzene (anhydrous, 98%) and chloroform (HPLC grade), used to form the polymer solutions, were acquired from Sigma-Aldrich and Fisher Scientific, respectively. The gold (Au wire, 99.99% pure) and silver (Ag wire, 99.99% pure) utilized in electrode deposition were purchased from Kurt J. Lesker Co. The PBDT-TTDPP polymer was synthesized as previously reported.[34]

2.2. Photodetector Development. ITO-coated glass substrates were sonicated in acetone and isopropanol for 10 min each, then

DOI: 10.1021/acsaelm.9b00597
ACS Appl. Electron. Mater. 2019, 1, 2455−2462

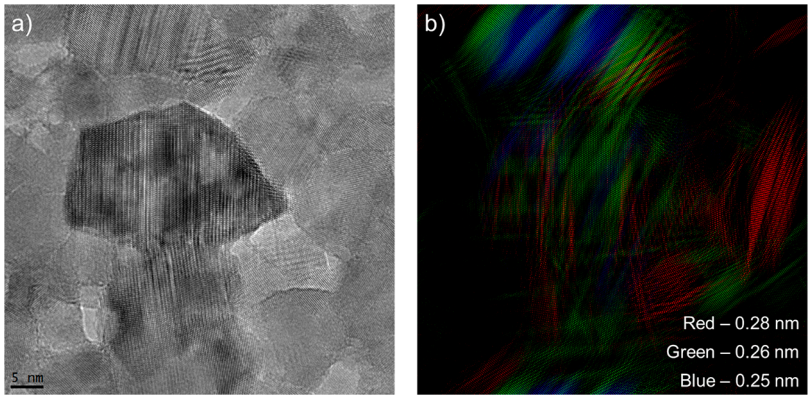

Figure 2. (a) Cross-sectional TEM image of a UV−ozone treated ZnO film. (b) Color map of the TEM image displaying oriented lattice spacing of the ZnO grains.

rinsed with DI water after, and dried with compressed nitrogen. Subsequently, the substrates were plasma cleaned for 10 min at a chamber pressure of 300 mTorr of O_2 gas in a Harrick Plasma PDC-32G plasma cleaner. The ZnO precursor solution was formed by dissolving 1 g of zinc acetate dihydrate in 10 mL of 2-methoxyethanol and adding 277 μL of ethanolamine. This solution was left to stir for at least 12 h. On the clean ITO-on-glass substrates, 0.5 mL of the ZnO solution was spin-cast at 2000 rpm for 60 s using a glass pipet. Once spin-casting was finished, the ZnO films were allowed to rest at room temperature for at least 5 min and subsequently transferred to a hot plate also at room temperature. Temperature on the hot plate was increased at a rate of 50 °C/min until 350 °C, at which the film was left to anneal for 50 min. This spin-casting procedure was repeated 8 times to attain the desired RMS roughness and film thickness of the ZnO. The hot plate was allowed to cool to room temperature between each layer of annealing. For the final layer of ZnO, the film was allowed to rest for 5 min after spin-casting and then prebaked for 2 min at 100 °C in an oven. After prebaking, the UV−ozone treatment was conducted on the film at an O_2 chamber pressure of 300 mTorr for 60 s. After UV−ozone treatment, the film was annealed at a rate of 50 °C/min until 350 °C and left for 50 min. Completed films were annealed overnight in an oven at 220 °C. All spin-casting and annealing steps were conducted in air.

Upon film completion, the ZnO films were transferred to a N_2 atmosphere glovebox (O_2 and H_2O < 5 ppm) for spin-casting of the organic polymer. The polymer solution was prepared by dissolving the polymer powder in a mixture of 1,2-dichlorobenzene and chloroform (1:1 vol %) in a concentration of 10 mg/mL for at least 8 h. The polymer was then spin-cast on the ZnO film using a spin speed of 680 rpm for 40 s and then annealed for 20 min at 130 °C. Upon completion of polymer annealing, 50 nm of gold was thermally evaporated at a pressure of 10^{-5} mbar onto the devices using an evaporation mask. The active areas of all devices were encapsulated under a glass coverslip using the Ossila epoxy, curing for 5 min under a UV lamp. Each individual device has an active area of 6.0 mm^2.

2.3. Characterization. Photodetector current−voltage measurements were conducted using a Keithley 2400 source meter. Responsivity was measured using a LabVIEW program that communicates with a Keithley 2400 source meter, Stanford Research Systems SR810 lock-in amplifier, and a CM110 1/8 m monochromator from Spectral Products. Response times for the photodetectors were measured using a chopper and 785 nm laser diode from Thorlabs and a Zurich Instruments MFLI lock-in amplifier.

TEM images of the ZnO films were taken using an FEI Tecnai F30 G2 Twin TEM at an accelerating voltage of 300 kV. Cross-sections of the ZnO films were formed by focused ion beam milling and polishing, using a FEI Scios DualBeam FIB SEM at various beam currents and accelerating voltages until the cross-sections were less than 100 nm in thickness. From these cross-sections, EELS spectra were collected in STEM mode at 300 kV and a 0.5 eV dispersion using a Quantum Gatan Imaging Filter CCD. SEM images were taken at an accelerating voltage of 5 kV, beam current of 0.1 nA, and a 10 μs dwell time. ZnO film thicknesses were found to be 250 nm, as indicated by TEM cross-sections.

X-ray diffraction (XRD) measurements were completed using a Bruker D8 Discover diffractometer with a copper anode (Kα = 1.54 Å). The UPS measurements were performed using a SPECS PHOIBOS 150 electron analyzer and a UVS-300-A UV lamp at a pressure below 2.0×10^{-10} mbar. The ZnO samples were annealed at 400 °C at a pressure lower than 2.0×10^{-9} mbar. The photon energy was 21.218 eV (He I), and the measurements were performed at room temperature. The energy resolution is 80 meV.

3. RESULTS AND DISCUSSION

3.1. ZnO Characterization. The sol−gel processed ZnO films were characterized by XRD and UPS to understand how the crystal structure and valence structure may change due to the passivation of V_O. Figure 1a shows the XRD data for treated and nontreated ZnO thin films grown on Si; no difference in structure is found between them. Along with the Si peaks, the Bragg reflections are indicative of a hexagonal wurtzite structure for ZnO. From a Le Bail fit, their lattice parameters were found to be $a = b = 3.24$ Å and $c = 5.19$ Å with the space group $P6_3mc$ (Figure 1b).

The UPS spectra of the treated and nontreated ZnO films are plotted in Figure 1c. The UPS spectra, which measure the DOS of the valence band, show two prominent peaks at 4.5 and 10.5 eV, which are from the O 2p orbitals (lone pair) and Zn 3d band, respectively.[35] In the UV−ozone treated sample, the peaks shift toward higher binding energies. Specifically, the two curves have the same shape, but the treated spectrum is shifted by 0.4 eV compared to the nontreated one. The spectral shift indicates that the UV−ozone treated sample is more resistive than the nontreated sample. Resistive films result in surface charging effects due to which the UPS spectrum shifts to higher binding energies. In addition, the higher O 2p peak of the treated sample can be attributed to a higher concentration of O near the surface of the UV−ozone treated sample.

To visualize film formation, cross-sectional TEM images were taken. Figure 2a shows a typical image of the ZnO cross-section, clearly indicating these films are composed of randomly oriented polycrystalline grains. These grains range in size from 5 to 20 nm, as seen in images at lower magnification. Using XRD data and a Fourier transform of the TEM data, we can produce a color map indicating aligned planes with a particular lattice spacing. The crystal at the center of Figure 2b appears to be polycrystalline, aligned parallel to

DOI: 10.1021/acsaelm.9b00597
ACS Appl. Electron. Mater. 2019, 1, 2455−2462

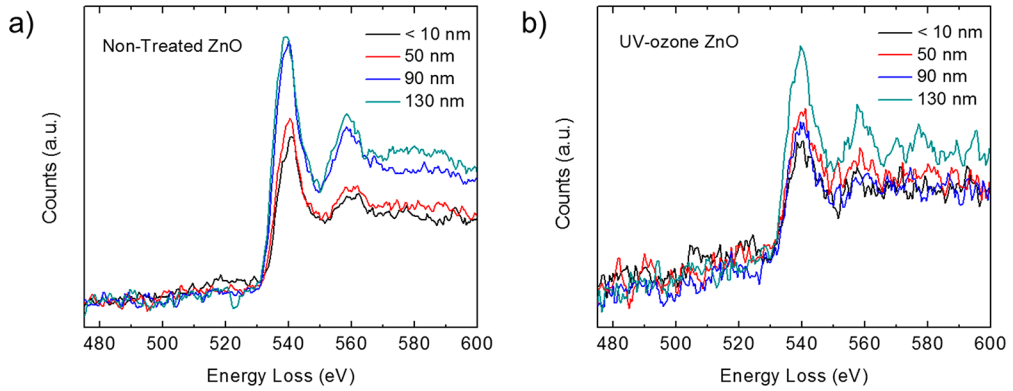

Figure 3. Electron energy loss spectra near the O K-edge from (a) nontreated ZnO and (b) UV−ozone treated ZnO cross-sections.

the (002) and (101) planes as indicated by the green and blue regions, respectively. The spacing indicated in Figure 2b was both measured within the TEM image and calculated from the lattice parameters found in Figure 1b from the XRD fitting. The lattice spacings obtained by the two methods are in good agreement with each other. Between the UV−ozone treated and nontreated films, there are no differences in structure, grain size, or crystal orientation.

In a previous study,[36] we have seen not only that the UV−ozone treatment fills the surface defects but it also permeates into the bulk of the film. The photoluminescence spectrum in that study indicated a decrease in V_O for UV−ozone treated ZnO films, which was inferred from a decrease in the defect emission at 525 nm compared to nontreated films. Concomitantly, a significant improvement in the performance of n-type field-effect transistors was observed for UV−ozone treated films compared to nontreated ZnO.[36] Since charge transport within a field-effect transistor occurs at the dielectric−semiconductor interface, one could estimate that V_O was filled at least 30 nm into the film.

The EELS spectra from ZnO cross-sectional films may be used to determine the interaction depth of the UV−ozone treatment. Figure 3 shows the EELS data from a nontreated and treated ZnO film at varying depths. Typically, the oxygen K-edge onset energy, where the incident beam electrons interact with the core O electrons, occurs at 532 eV. This onset is reliably observed in the UV−ozone treated ZnO film for the first 90 nm of film depth, as shown in Table 1. The energy resolution of the instrument is 0.5 eV. Beyond 110 nm, there is a small shift to lower energies in the K-edge onset. Meanwhile, the nontreated ZnO has an O K-edge onset at a lower energy throughout the depth of the film. In addition, the treated sample's full width at half-maximum (fwhm) of the O K-edge peak increases steadily from a depth of 30 to 130 nm, while the fwhm of the nontreated sample varies significantly. These results are tabulated in Table 1. EELS calculations from oxide materials, including ZnO, have indicated that the presence of V_O may shift the O K-edge onset to lower energy as well as broaden the peak due to more available states.[37,38] Those calculations along with the data presented in Figure 3 then suggest the UV−ozone treatment does indeed permeate into the bulk of the ZnO film and fills V_O. The exact interaction depth is difficult to conclude as the effect appears to be gradual. However, from the K-edge onset of the treated sample which consistently occurs at 532 eV, it appears that the treatment fills V_O at least 90 nm into the film.

Table 1. O K-Edge Onset Energies and Full Width at Half-Maximum of the Edge Structure for ZnO Films

	nontreated		UV−ozone	
film depth (nm)	O K-edge (eV)	fwhm (eV)	O K-edge (eV)	fwhm (eV)
<10	530.5	11.0	532	12.8
30	530	12.1	532	11.2
50	531	10.0	532	11.3
70	529	11.4	532	11.4
90	530.5	10.8	532	11.7
110	529	11.6	531	12.1
130	529	12.7	530	12.4
150	529	12.4	530	11.2
170	530.5		531	10.0

3.2. ZnO:DPP Photodiodes. Shifting from film characterization, these ZnO films were then applied in organic−inorganic hybrid photodiodes, utilizing a DPP-based donor−acceptor copolymer as the active layer. Panels a−c of Figure 4 illustrate the nanopatterned ZnO surface in ZnO:DPP photodetectors, including the device architecture and a schematic of the BDT-TTDPP copolymer used in this work. The film texturing increases the surface area, which yields higher device responsivities compared to less rough films.[2,3,15,16,34] Such textured films along with a p-type organic semiconductor thus allow a better charge dissociation and facilitate the use of these interfaces in photodiodes and solar cells even without the use of fullerenes.

Figure 5 shows the photoresponsivity of two ZnO−DPP photodiodes where all of the layers were identical except for the ZnO layer, which was UV−ozone treated in one and in the other was nontreated. Along with the responsivity, the absorption spectrum of BDT-TTDPP is also shown. The filling of V_O during the UV−ozone treatment in ZnO significantly improves the responsivity of the BDT-TTDPP:ZnO photodiodes (Figure 5). By filling vacancy sites, charge trapping is reduced at the DPP:ZnO interface, improving the exciton dissociation and reducing the dark current. Finding methods to decrease the dark current and the overall noise current in photodiodes, especially red and near-infrared photodiodes, is vital to optimize performance as thermal excitations can lead to high noise currents. We can further express the improvement in UV−ozone treated ZnO devices through the specific detectivity, $D^* = R/(2qJ_{dark})^{1/2}$, where R is the photoresponsivity, q is the fundamental charge, and J_{dark} is the dark current density. This approximation assumes the shot noise is the dominant source of noise in a

DOI: 10.1021/acsaelm.9b00597
ACS Appl. Electron. Mater. 2019, 1, 2455−2462

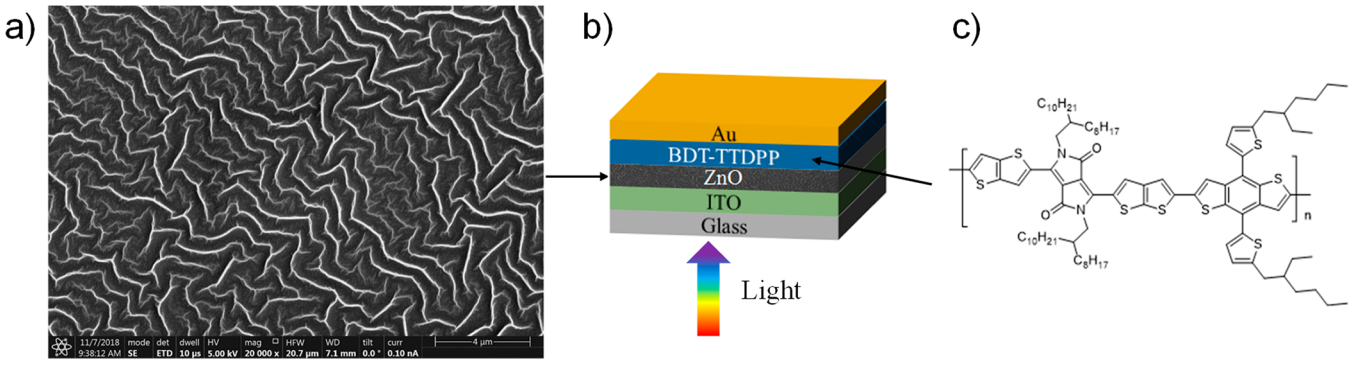

Figure 4. (a) SEM image of the nanopatterned ZnO film with a horizontal field width of 20.7 μm. The scale bar in the lower right corner is 4 μm. (b) Photodetector architecture of the devices used in this work, including illumination direction, and (c) schematic of the BDT-TTDPP copolymer used in conjunction with ZnO.

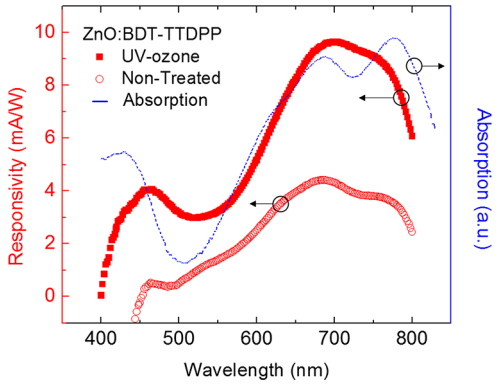

Figure 5. Responsivity data from BDT-TTDPP diodes using UV−ozone treated and nontreated ZnO. The BDT-TTDPP absorption data are the dashed blue line. Responsivity measurements were taken at 0 V bias.

device. However, we note that when detectivities are greater than 10^{11}Jones, it is of particular importance that detectivity is obtained from $D^* = (A\Delta f)^{1/2}/\mathrm{NEP}$, where A is the device area, Δf is the electrical bandwidth, and NEP is the noise equivalent power.[39] The noise equivalent power takes into account the total noise in a device, composed of shot noise, thermal noise, and flicker noise. Here, we used the shot noise approximation to determine the specific detectivity of the photodiodes. Average values and best values (in parentheses) for the ZnO:DPP devices are provided in Table 2. On average, across more than 15 devices, the specific detectivity of the treated ZnO diodes is more than double its nontreated counterpart.

In addition, a PEDOT:PSS buffer layer was added between the DPP polymer and the electrode in a different device. A buffer layer can reduce the dark current and improve device performance. As seen in Table 2, introduction of the PEDOT:PSS layer slightly improves the specific detectivity but does not really improve the responsivity compared to the UV−ozone treated photodiode without the buffer layer.

Table 2. Average Values for BDT-TTDPP:ZnO Photodiodes with Best Values in Parentheses

structure	responsivity (mA/W)	J_{dark} (A/cm^2)	D^* (Jones)
ITO/ZnO (nontreated)/ BDT-TTDPP/Au	2.4 (4.4)	7.5×10^{-8} (3.5×10^{-8})	1.6×10^{10} (2.9×10^{10})
ITO/ZnO (UV−ozone)/ BDT-TTDPP/Au	4.2 (9.7)	3.7×10^{-8} (7.9×10^{-9})	3.7×10^{10} (6.9×10^{10})
ITO/ZnO (UV−ozone)/ BDT- TTDPP/ PEDOT:PSS/Ag	4.1 (4.7)	2.4×10^{-8} (1.1×10^{-8})	5.3×10^{10} (6.8×10^{10})

While treating the ZnO film led to improvements in specific detectivities, the diode response times seem to be independent of the UV−ozone treatment. Response times are expressed as the rise time (τ_r) and the decay time (τ_d), where τ_r is defined as the time it takes for the photocurrent in a device to increase from 10% to 90% of the maximum photocurrent upon excitation from an incident light signal with respect to the dark current. Likewise, the decay time is the time it takes for the photocurrent to decrease from 90% to 10% of the maximum photocurrent. Figure 6 shows response time curves for both nontreated and treated ZnO:DPP diodes. The diodes were excited with a 785 nm laser diode source, and the incident light was modulated by a chopper at 50 Hz. In nontreated devices, τ_r and τ_d are 3.2 and 3.5 ms, respectively. In treated devices, response times are about the same with τ_r and τ_d being 3.3 and 3.4 ms, respectively. The introduction of a PEDOT:PSS buffer layer results in similar response times with rise and decay times being 3.2 and 3.6 ms, respectively.

The DPP-based diodes shown in this work perform well without the use of fullerenes. Undoubtedly, using fullerene materials to better dissociate excitons and incorporating additional buffer layers would improve device performances, as has been demonstrated in a previous work.[34] However, blending fullerenes with other semiconductors has been shown to complicate optical responses.[24] Table 3 shows values from other works using a DPP-based material as the photoactive layer with similar device architectures, keeping in mind that the DPP layer has been blended with PCBM in the referenced literature. When compared to other DPP:PCBM blended systems, the architecture of textured ZnO with the UV−ozone treatment used in this work shows significant promise for photodiode application.

4. CONCLUSIONS

Reducing recombination centers in photodetectors is vital in order to improve exciton dissociation and decreasing dark currents. UV−ozone treatment of ZnO films in hybrid organic−inorganic systems is a simple and cost-efficient method for enhancing device performance. The UV−ozone treatment does not noticeably alter the crystal structure in ZnO but results in a less conductive film with a higher oxygen concentration, as shown by UPS. This is also more than a surface treatment; EELS suggests oxygen vacancy sites are

DOI: 10.1021/acsaelm.9b00597
ACS Appl. Electron. Mater. 2019, 1, 2455−2462

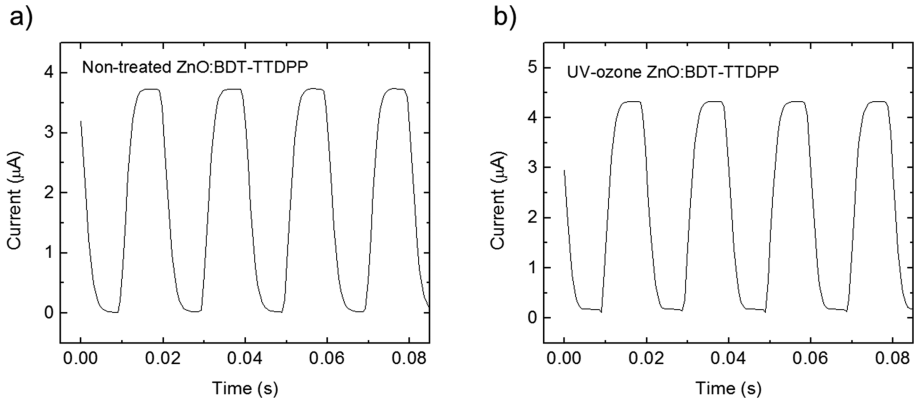

Figure 6. Response time measurements from (a) nontreated ZnO:TTDPP and (b) UV−ozone treated photodiodes.

Table 3. Device Architectures and Figures of Merit from DPP:ZnO Photodiodes

structure	responsivity (mA/W)	J_{dark} (A/cm^2) (at V_{bias} (V))	D^* (Jones)	ref
ITO/ZnO (nontreated)/BDT- TTDPP/Au	4.4	3.5×10^{-8} (0)	2.9×10^{10}	this work
ITO/ZnO (UV−ozone)/BDT- TTDPP/Au	9.7	7.9×10^{-9} (0)	6.9×10^{10}	this work
ITO/ZnO (UV−ozone)/BDT- TTDPP/PEDOT:PSS/Ag	4.7	1.1×10^{-8} (0)	6.8×10^{10}	this work
ITO/PEDOT:PSS/BDT- TTDPP:PCBM/Ca/Al	160	NR	2.1×10^{12}	34
ITO/ZnO/PDPP-FBT:PCBM/MoO_x/Ag	11.5	1.2×10^{-8} (−0.5)	3.2×10^{11}	40
ITO/PBDTT-DPP:PCBM/MoO_3/Ag	50	2.1×10^{-11} (0)	2.0×10^{13}	41
ITO/PEIE/PMDPP3T:PCBM/PEDOT:PSS	370	3.0×10^{-9} (−0.2)	1.2×10^{13}	42
ITO/PEIE/PMDPP3T:PCBM/MoO_3/Ag	NR	6.0×10^{-6} (−0.2)	3.0×10^{11}	42
ITO/PEDOT:PSS/(P1) PDPP:PCBM/BCP/Al	20.8	1.4×10^{-9} (−0.1)	4.6×10^{11}	43
ITO/PEDOT:PSS/(P3) PDPP-TIIG:PCBM/BCP/Al	2.4	1.5×10^{-8} (−0.1)	2.3×10^{10}	43

passivated within the bulk of the film at least to 90 nm. Using a DPP-based p-type polymer, BDT-TTDPP, as the absorbing layer with ZnO as the electron acceptor and transport layer in photodetector architectures, we have shown improved performances when the ZnO film is UV−ozone treated. On average, responsivities nearly double and dark currents are halved due to this simple treatment when compared to nontreated devices. In best performing treated devices, specific detectivities are more than double those of the nontreated devices. When compared to other DPP-based photodiodes, the devices reported here work well as fullerene-free devices with specific detectivities as high as 6.9×10^{10} Jones. We suggest adopting this simple UV−ozone treatment process due to its facile use and prominent benefits for organic photodiodes utilizing ZnO as an electron transport layer.

AUTHOR INFORMATION

Corresponding Author

*E-mail: guhas@missouri.edu.

ORCID

Satish Patil: 0000-0003-3884-114X

Suchismita Guha: 0000-0002-6269-2298

Present Address

[‖]Department of Chemistry, Presidency University, 86/1 College Street, Kolkata 73, India.

Notes

The authors declare no competing financial interest.

ACKNOWLEDGMENTS

We acknowledge the support of this work through the U.S. National Science Foundation (NSF) under Grant No. ECCS-1707588. S.P. thanks the Department of Science and Technology, New Delhi, India for the Swarnajayanti fellowship. G.B. was supported by the U.S. NSF under Grant No. DMR-1809160. A.P. thanks the University of Missouri—Columbia Electron Microscopy Core Facility for providing instrument time via the Excellence in Electron Microscopy Award. We thank Dr. Sorb Yesudhas for valuable discussions and fitting of the XRD data.

REFERENCES

(1) Zhang, Y.-X.; Fang, J.; Li, W.; Shen, Y.; Chen, J.-D.; Li, Y.; Gu, H.; Pelivani, S.; Zhang, M.; Li, Y.; Tang, J.-X. Synergetic Transparent Electrode Architecture for Efficient Non-Fullerene Flexible Organic Solar Cells with > 12% Efficiency. *ACS Nano* **2019**, *13*, 4686−4694.

(2) Morvillo, P.; Diana, R.; Mucci, A.; Bobeico, E.; Ricciardi, R.; Minarini, C. Influence of Annealing Treatments on Solution-Processed ZnO Film Deposited on ITO Substrate as Electron Transport Layer for Inverted Polymer Solar Cells. *Sol. Energy Mater. Sol. Cells* **2015**, *141*, 210−217.

(3) Richardson, B. J.; Wang, X.; Almutairi, A.; Yu, Q. High Efficiency PTB7-Based Inverted Organic Photovoltaics on Nano-Ridged and Planar Zinc Oxide Electron Transport Layers. *J. Mater. Chem. A* **2015**, *3*, 5563−5571.

(4) Ko, S. H.; Lee, D.; Kang, H. W.; Nam, K. H.; Yeo, J. Y.; Hong, S. J.; Grigoropoulos, C. P.; Sung, H. J. Nanoforest of Hydrothermally Grown Hierarchical ZnO Nanowires for a High Efficiency Dye-Sensitized Solar Cell. *Nano Lett.* **2011**, *11*, 666−671.

(5) Bolink, H. J.; Coronado, E.; Sessolo, M. White Hybrid Organic-Inorganic Light-Emitting Diode Using ZnO as the Air-Stable Cathode. *Chem. Mater.* **2009**, *21*, 439−441.

(6) Wang, C.; Bao, R.; Zhao, K.; Zhang, T.; Dong, L.; Pan, C. Enhanced emission intensity of vertical aligned flexible ZnO nanowire/p-polymer hybridized LED array by piezo-phototronic effect. *Nano Energy* **2015**, *14*, 364−371.

(7) Smith, J.; Bashir, A.; Adamopoulos, G.; Anthony, J. E.; Bradley, D. D. C.; Heeney, M.; McCulloch, I.; Anthopoulos, T. D. Air-Stable

DOI: 10.1021/acsaelm.9b00597
ACS Appl. Electron. Mater. 2019, 1, 2455−2462

Solution-Processed Hybrid Transistors with Hole and Electron Mobilities Exceeding 2 cm^2 V^{-1} s^{-1}. *Adv. Mater.* **2010**, *22*, 3598−3602.
(8) Anta, J. A.; Guillén, E.; Tena-Zaera, R. ZnO-Based Dye-Sensitized Solar Cells. *J. Phys. Chem. C* **2012**, *116*, 11413−11425.
(9) Tributsch, H.; Calvin, M. Electrochemistry of Excited Molecules: Photo-Electrochemical Reactions of Chlorophylls. *Photochem. Photobiol.* **1971**, *14*, 95−112.
(10) Janotti, A.; Van de Walle, C. G. Fundamentals of Zinc Oxide as a Semiconductor. *Rep. Prog. Phys.* **2009**, *72*, 126501.
(11) Wang, J.; Chen, R.; Xiang, L.; Komarneni, S. Synthesis, Properties and Applications of ZnO Nanomaterials with Oxygen Vacancies: A Review. *Ceram. Int.* **2018**, *44*, 7357−7377.
(12) Pelicano, C. M.; Yanagi, H. pH-controlled surface engineering of nanostructured ZnO films generated via a sustainable low-temperature H2O oxidation process. *Appl. Surf. Sci.* **2019**, *467*−*468*, 932−939.
(13) Sahdan, M. Z.; Malek, M. F.; Alias, M. S.; Kamaruddin, S. A.; Norhidayah, C. A.; Sarip, N.; Nafarizal, N.; Rusop, M. Fabrication of inverted bulk heterojunction organic solar cells based on conjugated P3HT:PCBM using various thicknesses of ZnO buffer layer. *Optik* **2015**, *126*, 645−648.
(14) Vasilopoulou, M.; Konofaos, N.; Davazoglou, D.; Argitis, P.; Stathopoulos, N. A.; Savaidis, S. P.; Iliadis, A. A. Organic Photovoltaic Performance Improvement Using Atomic Layer Deposited ZnO Electron-Collecting Layers. *Solid-State Electron.* **2014**, *101*, 50−56.
(15) Park, H.-Y.; Lim, D.; Kim, K.-D.; Jang, S.-Y. Performance Optimization of Low-Temperature-Annealed Solution-Processable ZnO Buffer Layers for Inverted Polymer Solar Cells. *J. Mater. Chem. A* **2013**, *1*, 6327−6334.
(16) Sekine, N.; Chou, C.-H.; Kwan, W. L.; Yang, Y. ZnO Nano-Ridge Structure and its Application in Inverted Polymer Solar Cell. *Org. Electron.* **2009**, *10*, 1473−1477.
(17) Prosa, M.; Tessarolo, M.; Bolognesi, M.; Margeat, O.; Gedefaw, D.; Gaceur, M.; Videlot-Ackermann, C.; Andersson, M. R.; Muccini, M.; Seri, M.; Ackermann, J. Enhanced Ultraviolet Stability of Air-Processed Polymer Solar Cells by Al Doping of the ZnO Interlayer. *ACS Appl. Mater. Interfaces* **2016**, *8*, 1635−1643.
(18) Chen, D.; Wang, Z.; Ren, T.; Ding, H.; Yao, W.; Zong, R.; Zhu, Y. Influence of Defects on the Photocatalytic Activity of ZnO. *J. Phys. Chem. C* **2014**, *118*, 15300−15307.
(19) Wang, J.; Wang, Z.; Huang, B.; Ma, Y.; Liu, Y.; Qin, X.; Zhang, X.; Dai, Y. Oxygen Vacancy Induced Band-Gap Narrowing and Enhanced Visible Light Photocatalytic Activity of ZnO. *ACS Appl. Mater. Interfaces* **2012**, *4*, 4024−4030.
(20) Kim, K.-D.; Lim, D. C.; Hu, J.; Kwon, J.-D.; Jeong, M.-G.; Seo, H. O.; Lee, J. Y.; Jang, K.-Y.; Lim, J.-H.; Lee, K. H.; Jeong, Y.; Kim, Y. D.; Cho, S. Surface Modification of a ZnO Electron-Collecting Layer Using Atomic Layer Deposition to Fabricate High-Performing Inverted Organic Photovoltaics. *ACS Appl. Mater. Interfaces* **2013**, *5*, 8718−8723.
(21) Bao, Q.; Liu, X.; Xia, Y.; Gao, F.; Kauffmann, L.-D.; Margeat, O.; Ackermann, J.; Fahlman, M. Effects of Ultraviolet Soaking on Surface Electronic Structures of Solution Processed ZnO Nanoparticle Films in Polymer Solar Cells. *J. Mater. Chem. A* **2014**, *2*, 17676−17682.
(22) Mahmud, M. A.; Elumalai, N. K.; Upama, M. B.; Wang, D.; Gonçales, V. R.; Wright, M.; Xu, C.; Haque, F.; Uddin, A. Passivation of Interstitial and Vacancy Mediated Trap-states for Efficient and Stable Triple-Cation Perovskite Solar Cells. *J. Power Sources* **2018**, *383*, 59−71.
(23) Li, D.; Qin, W.; Zhang, S.; Liu, D.; Yu, Z.; Mao, J.; Wu, L.; Yang, L.; Yin, S. Effect of UV-Ozone Process on the ZnO Interlayer in the Inverted Organic Solar Cells. *RSC Adv.* **2017**, *7*, 6040−6045.
(24) García de Arquer, F. P.; Armin, A.; Meredith, P.; Sargent, E. H. Solution-Processed Semiconductors for Next-Generation Photodetectors. *Nat. Rev. Mater.* **2017**, *2*, 16100.
(25) Chen, B.; Yang, Y.; Cheng, P.; Chen, X.; Zhan, X.; Qin, J. Designing a Thiophene-Fused DPP Unit to Build an A-D-A Molecule for Solution-Processed Solar Cells. *J. Mater. Chem. A* **2015**, *3*, 6894−6900.
(26) Liu, J.; Sun, Y.; Moonsin, P.; Kuik, M.; Proctor, C. M.; Lin, J.; Hsu, B. B.; Promarak, V.; Heeger, A. J.; Nguyen, T.-Q. Tri-Diketopyrrolopyrrole Molecular Donor Materials for High-Performance Solution-Processed Bulk Heterojunction Solar Cells. *Adv. Mater.* **2013**, *25*, 5898−5903.
(27) Naik, M. A.; Patil, S. Diketopyrrolopyrrole-Based Conjugated Polymers and Small Molecules for Organic Ambipolar Transistors and Solar Cells. *J. Polym. Sci., Part A: Polym. Chem.* **2013**, *51*, 4241−4260.
(28) Kanimozhi, C.; Yaacobi-Gross, N.; Chou, K. W.; Amassian, A.; Anthopoulos, T. D.; Patil, S. Diketopyrrolopyrrole-Diketopyrrolopyrrole-Based Conjugated Copolymer for High-Mobility Organic Field-Effect Transistors. *J. Am. Chem. Soc.* **2012**, *134*, 16532−16535.
(29) Li, J.; Zhao, Y.; Tan, H. S.; Guo, Y.; Di, C.-A.; Yu, G.; Liu, Y.; Lin, M.; Lim, S. H.; Zhou, Y.; Su, H.; Ong, B. S. A Stable Solution-Processed Polymer Semiconductor with Record High-Mobility for Printed Transistors. *Sci. Rep.* **2012**, *2*, 754.
(30) Mukhopadhyay, T.; Puttaraju, B.; Senanayak, S. P.; Sadhanala, A.; Friend, R.; Faber, H. A.; Anthopoulos, T. D.; Salzner, U.; Meyer, A.; Patil, S. Air-Stable n-channel Diketopyrrolopyrrole-Diketopyrrolopyrrole Oligomers for High Performance Ambipolar Organic Transistors. *ACS Appl. Mater. Interfaces* **2016**, *8*, 25415−25427.
(31) Senanayak, S. P.; Ashar, A. Z.; Kanimozhi, C.; Patil, S.; Narayan, K. S. Room-Temperature Bandlike Transport and Hall Effect in a High-Mobility Ambipolar Polymer. *Phys. Rev. B: Condens. Matter Mater. Phys.* **2015**, *91*, 115302.
(32) Sonar, P.; Singh, S. P.; Li, Y.; Soh, M. S.; Dodabalapur, A. A Low-Bandgap Diketopyrrolopyrrole-Benzothiadiazole-Based Copolymer for High-Mobility Ambipolar Organic Thin-Film Transistors. *Adv. Mater.* **2010**, *22*, 5409−5413.
(33) Zhang, Y.; Kim, C.; Lin, J.; Nguyen, T.-Q. Solution-Processed Ambipolar Field-Effect Transistor Based on Diketopyrrolopyrrole Functionalized with Benzothiadiazole. *Adv. Funct. Mater.* **2012**, *22*, 97−105.
(34) Pickett, A.; Mohapatra, A.; Laudari, A.; Khanra, S.; Ram, T.; Patil, S.; Guha, S. Hybrid ZnO-organic Semiconductor Interfaces in Photodetectors: A Comparison of Two Near-Infrared Donor-Acceptor Copolymers. *Org. Electron.* **2017**, *45*, 115−123.
(35) Schmerl, N. M.; Gentle, A. R.; Quinton, J. S.; Smith, G. B.; Andersson, G. G. Surface and Near Surface Area Density of States for Magnetron-Sputtered ZnO and Al-ZnO: A MIES, UPS, and VBXPS Study Investigating Ultrahigh Vacuum Sputter Cleaning and UV Oxygen Plasma. *J. Phys. Chem. C* **2016**, *120*, 15772−15784.
(36) Pickett, A.; Mohapatra, A. A.; Ray, S.; Robledo, C.; Ghosh, K.; Patil, S.; Guha, S. Interfacial Effects of UV-Ozone Treated Sol-Gel Processable ZnO for Hybrid Photodetectors and Thin Film Transistors. *MRS Adv.* **2019**, *4*, 1793−1800.
(37) Dileep, K.; Panchakarla, L. S.; Balasubramanian, K.; Waghmare, U. V.; Datta, R. Electron Energy Loss Spectroscopy of ZnO Nanocrystals with Different Oxygen Vacancy Concentrations. *J. Appl. Phys.* **2011**, *109*, 063523.
(38) Torruella, P.; Coll, C.; Martín, G.; López-Conesa, L.; Vila, M.; Díaz-Guerra, C.; Varela, M.; Ruiz-González, M. L.; Piqueras, J.; Peiró, F.; Estradé, S. Assessing Oxygen Vacancies in Bismuth Oxide through EELS Measurements and DFT Simulations. *J. Phys. Chem. C* **2017**, *121*, 24809−24815.
(39) Fang, Y.; Armin, A.; Meredith, P.; Huang, J. Accurate characterization of next-generation thin-film photodetectors. *Nat. Photonics* **2019**, *13*, 1−4.
(40) Lee, D. W.; Kang, Y.; Jo, B. H.; Jeon, G. G.; Park, J.; Yoon, S. E.; Zheng, J.; Ahn, T. K.; Park, H. J.; Kim, B.-G.; Kim, J. H. Morphology and Charge Recombination Effects on the Performance of Near-Infrared Photodetectors Based on Conjugated Polymers. *Org. Electron.* **2019**, *64*, 274−279.
(41) Nie, R.; Deng, X.; Feng, L.; Hu, G.; Wang, Y.; Yu, G.; Xu, J. Highly Sensitive and Broadband Organic Photodetectors with Fast Speed Gain and Large Linear Dynamic Range at Low Forward Bias. *Small* **2017**, *13*, 1603260.

DOI: 10.1021/acsaelm.9b00597
ACS Appl. Electron. Mater. 2019, 1, 2455−2462

(42) Xiong, S.; Tong, J.; Mao, L.; Li, Z.; Qin, F.; Jiang, F.; Meng, W.; Liu, T.; Li, W.; Zhou, Y. Double-Side Responsive Polymer Near-Infrared Photodetectors with Transfer-Printed Electrode. *J. Mater. Chem. C* **2016**, *4*, 1414−1419.
(43) Qi, J.; Han, J.; Zhou, X.; Yang, D.; Zhang, J.; Qiao, W.; Ma, D.; Wang, Z. Y. Optimization of Broad-Response and High-Detectivity Polymer Photodetectors by Bandgap Engineering of Weak Donor-Strong Acceptor Polymers. *Macromolecules* **2015**, *48*, 3941−3948.

DOI: 10.1021/acsaelm.9b00597
ACS Appl. Electron. Mater. 2019, 1, 2455−2462